

Remote sensing of snow grain-size and impurities from Airborne Multispectral Scanner data using a snow bidirectional reflectance distribution function model

TOMONORI TANIKAWA,¹ TERUO AOKI,² FUMIHIKO NISHIO³

¹*Graduate School of Life and Environmental Sciences, University of Tsukuba, Ibaraki 305-8571, Japan*

²*Meteorological Research Institute, Ibaraki 305-0052, Japan*

³*Center for Environmental Remote Sensing, Chiba University, Chiba 263-8522, Japan*

ABSTRACT. Algorithms to retrieve the snow grain-size and the concentration of snow impurities were developed using a theoretical bidirectional reflectance distribution function (BRDF) model of the snow surface. In this model, snow grains are assumed to be independent spherical ice particles, and the BRDF is calculated with multiple scattering by snow particles. Using these algorithms, the snow grain-size and snow impurities were retrieved from Airborne Multispectral Scanner (AMSS) images at the visible ($\lambda = 0.545 \mu\text{m}$) and near-infrared ($\lambda = 1.24, 1.64$ and $2.23 \mu\text{m}$) wavelengths observed over the flat snowfield in eastern Hokkaido, Japan, in February 1998. The estimated snow grain-size and impurities were consistent with the results of in situ measurements on the snow surface. For snow grain-size, measured reflectances in the different near-infrared AMSS channels indicated grain-size differences in the vertical profile of the snowpack.

INTRODUCTION

The large seasonal variation of snow-covered areas and very high snow albedos play a significant role in the Earth's radiation balance, making the cryosphere act as a cold source on the global scale. The snow albedo in the visible region depends strongly on the concentration of impurities (Warren and Wiscombe, 1980). These effects could cause an increase in the melting rate of snow in cold regions. The snow albedo in the visible region is reduced by 0.005–0.028 for fine-grained snow and by 0.015–0.08 for coarse-grained snow, with the observed concentration of soot, which is the most sensitive absorptive constituent of the Arctic snowpack, originating from Arctic haze (Warren and Clarke, 1986). On the other hand, the albedo in the near-infrared region depends on the near-surface snow grain-size (Wiscombe and Warren, 1980). Spatial and temporal changes in near-surface snow grain-size can help characterize the thermal history of the snowpack because the rate of grain growth is exponentially proportional to snow temperature (Jordan, 1991). Therefore, estimation of these parameters is important in monitoring the climate change in the cryosphere.

Remote sensing, using visible and near-infrared wavelengths, is one of the most suitable techniques for monitoring snow parameters at regional and global scales. For example, Sydor and others (1979) retrieved the dustfall from Landsat Multispectral Scanner (MSS) data, but the sensor accuracy was not sufficient for detailed work. Bourdelles and Fily (1993) and Fily and others (1997) retrieved snow grain-size from Landsat Thematic Mapper (TM) data, and Nolin and Dozier (1993, 2000) retrieved it from Airborne Visible/Infrared Imaging Spectrometer (AVIRIS) data. In these studies, the snow reflectance in the near-infrared regions that was calculated with the radiative transfer model was a function

of equivalent grain-size for solar incident angle. The effects of snow impurities have not been considered in these models because snowpacks at observation sites were very clean. However, the snow reflectance in the near-infrared region is affected by the presence of absorbing impurities as well as snow grain-size (Warren and Wiscombe, 1980). For example, in snowfields such as Barrow in Alaska, U.S.A., and Hokkaido in Japan, high concentrations of snow impurities were observed (Aoki and others, 1998, 2000), and snow-grain retrieval must take account of the effect of snow impurities.

Field experiments have shown the high anisotropic reflectance of snow (Grenfell and others, 1994; Aoki and others, 2000). The satellite sensor collects only a small portion of the energy reflected in all directions from a surface such as a snowfield. The assumption of isotropic reflectance of snow is too simple to retrieve the snow physical parameters, the results of which may contain large errors because the effects of bidirectional reflectance are generally not considered nor well corrected. Recently a digital elevation model has been used in the retrieval of snow grain-size (Nolin and Dozier, 1993). Nolin and Liang (2000) demonstrated the use of bidirectional reflectance modeling and surface particulate media modeling approaches for snow and soils. Therefore, we need to consider anisotropic snow-reflectance properties to retrieve the snow physical parameters from remote-sensing data.

The objective of this study is to develop an algorithm, the bidirectional reflectance distribution function (BRDF), which takes into account the anisotropic reflectance of snow surface in determining the snow grain-size and the concentration of impurities. Using Airborne Multispectral Scanner (AMSS) data at the visible and near-infrared wavelengths, these snow parameters are retrieved and we verified the algorithm from the AMSS data and in situ snow-pit measurements.

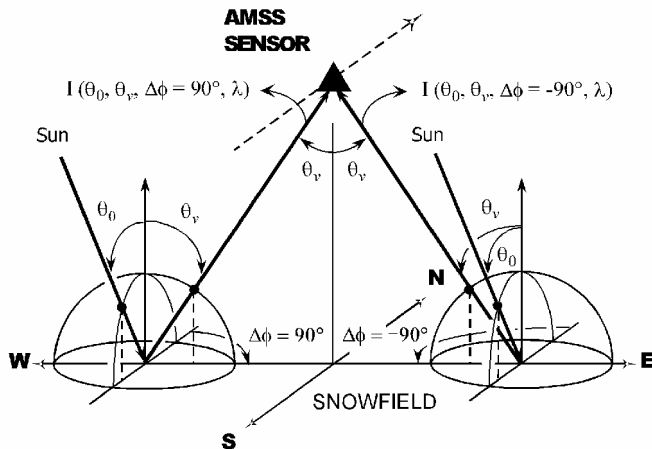


Fig. 1. Coordinate systems for the observations by the AMSS sensor. The symbols θ_0 and θ_v are the solar zenith angle and the viewing angle from the sensor, respectively; $\Delta\phi$ is the relative azimuth angle of the viewing direction from the solar direction. AMSS flew from south to north and observed the upward reflected radiance $I(\theta_0, \theta_v, \Delta\phi, \lambda)$ from the snow surface.

AMSS AND FIELD DATA

AMSS is an optical sensor installed on an aircraft which observes the radiance reflected from snow surface. This instrument acquires high-spatial-resolution images at 46 spectral channels in the wavelength region ranging from 0.40 to 12.45 μm with a swath angle of $\pm 35^\circ$. AMSS is developed as a preparatory simulator of the spaceborne optical sensors and to validate the remote-sensing algorithms with optical sensors such as the Advanced Earth Observing Satellite-II/Global Imager (ADEOS-II/GLI). In this study, the wavelengths (bandwidth) of AMSS selected to retrieve the snow physical parameters were 0.545 μm (0.541–0.550 μm) in the visible regions and 1.24 μm (1.23–1.25 μm), 1.64 μm (1.52–1.74 μm) and

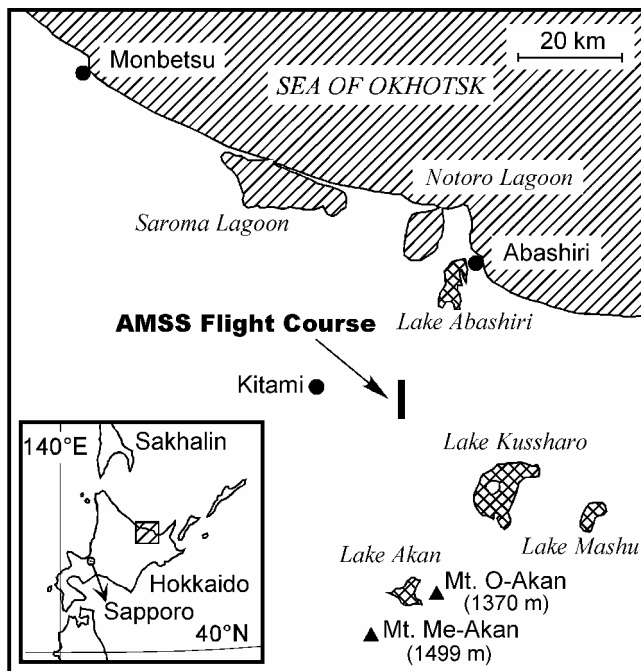


Fig. 2. Map showing the locations of the AMSS flight course in eastern Hokkaido. The AMSS observation was made at 1100 h LT, 25 February 1998. Solar zenith angle θ_0 was 53.5° .

2.23 μm (2.13–2.33 μm) in the near-infrared regions. Figure 1 shows the coordinate system for the AMSS observation.

The AMSS observations were made on the flat snowfield of eastern Hokkaido (Fig. 2), at 1100 h local time (LT) on 25 February 1998, when the solar zenith angle was 53.5° at approximately local solar noon. The flight course was from south to north, and the spatial resolution was about 1.2×2.0 m at nadir with an aircraft height of 930 m and a ground speed of 280 km h^{-1} .

February 25, 1998
 Observed at 09:15 - 10:30 LT
 Air temperature = -9.9°C at 09:20 LT

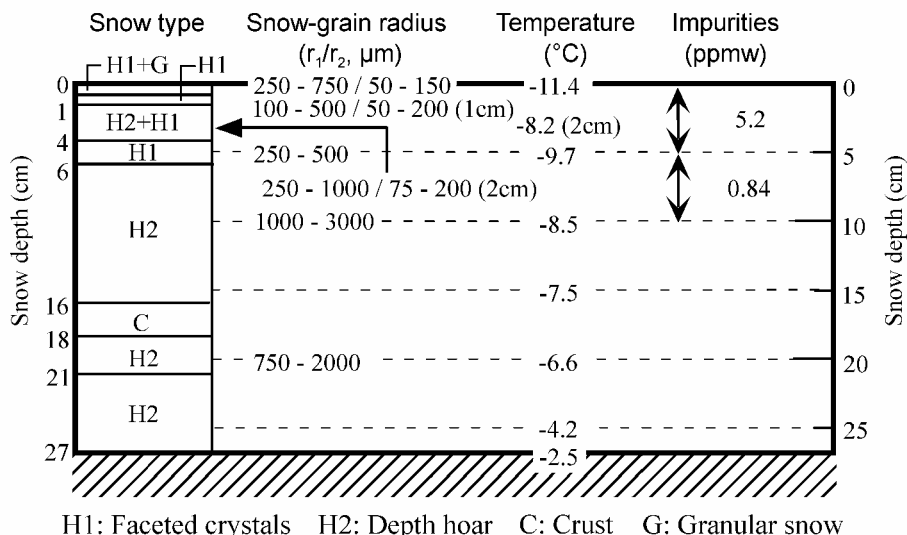


Fig. 3. Vertical profiles of snow parameters observed from snow-pit work on 25 February 1998. Snow grain-sizes (radius) were measured with about 10 μm resolution using a hand-held lens. There were two kinds of dimensions of grain-sizes: one was one-half the length of the major axis of crystals or dendrites (r_1), and the other was one-half the branch width of dendrites or one-half the dimension of the narrower portion of broken crystals (r_2). Snow impurities were collected on the Nuclepore filters, and the concentration was estimated with a balance.

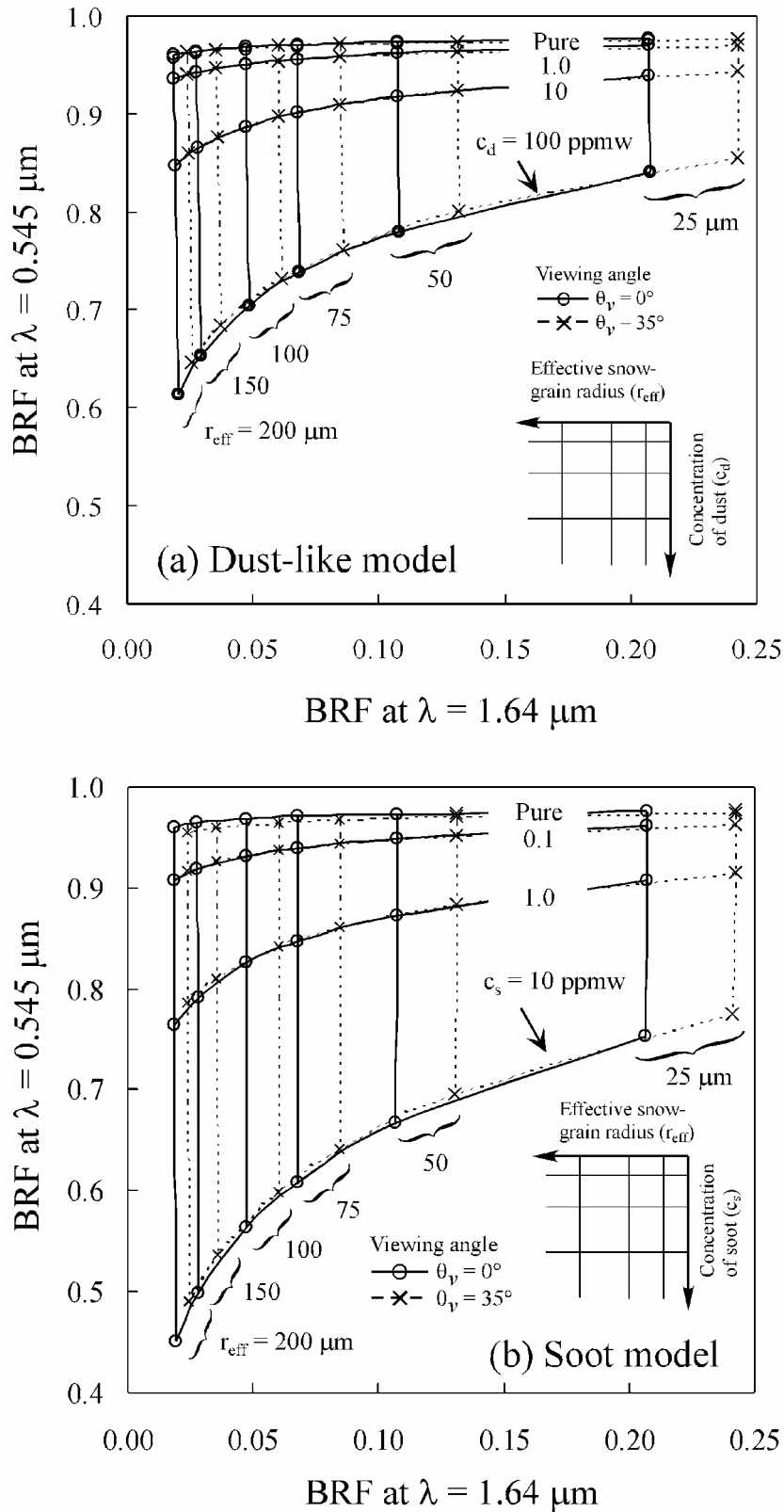


Fig. 4. The relationships of theoretical BRFs between the visible ($\lambda = 0.545 \mu\text{m}$) and the near-infrared ($\lambda = 1.64 \mu\text{m}$) wavelengths as functions of the concentration of snow impurities (c_d and c_s) and the effective snow-grain radius (r_{eff}). For snow impurities, (a) dust-like and (b) soot particles are assumed to contain snow particles as an external mixture. Thick lines indicate BRFs for the viewing angle $\theta_v = 0^\circ$ (nadir), and broken lines the maximum viewing angles $\theta_v = 35^\circ$.

Figure 3 shows the results of snow-pit work coincident with the AMSS observation. The sky condition was clear and the air temperature was -9.9°C at 0920 h LT. Before the AMSS observation, a 10 cm new snowfall was observed on 20 February, and on 21 February a new snowfall of < 1 cm was measured. The snow depth was 27 cm, the snow types at the snow surface consisted of faceted crystals and

granular snow, and those of lower parts were depth hoar and crust. The snowpack temperature was below freezing and there was no free water in the snowpack. The measured snow grain-sizes in deep layers were larger than those at the surface. Aoki and others (2000), using the results of the same snow-pit work, concluded that the optically equivalent snow grain-size was not the geometric radius (r_1) but the branch

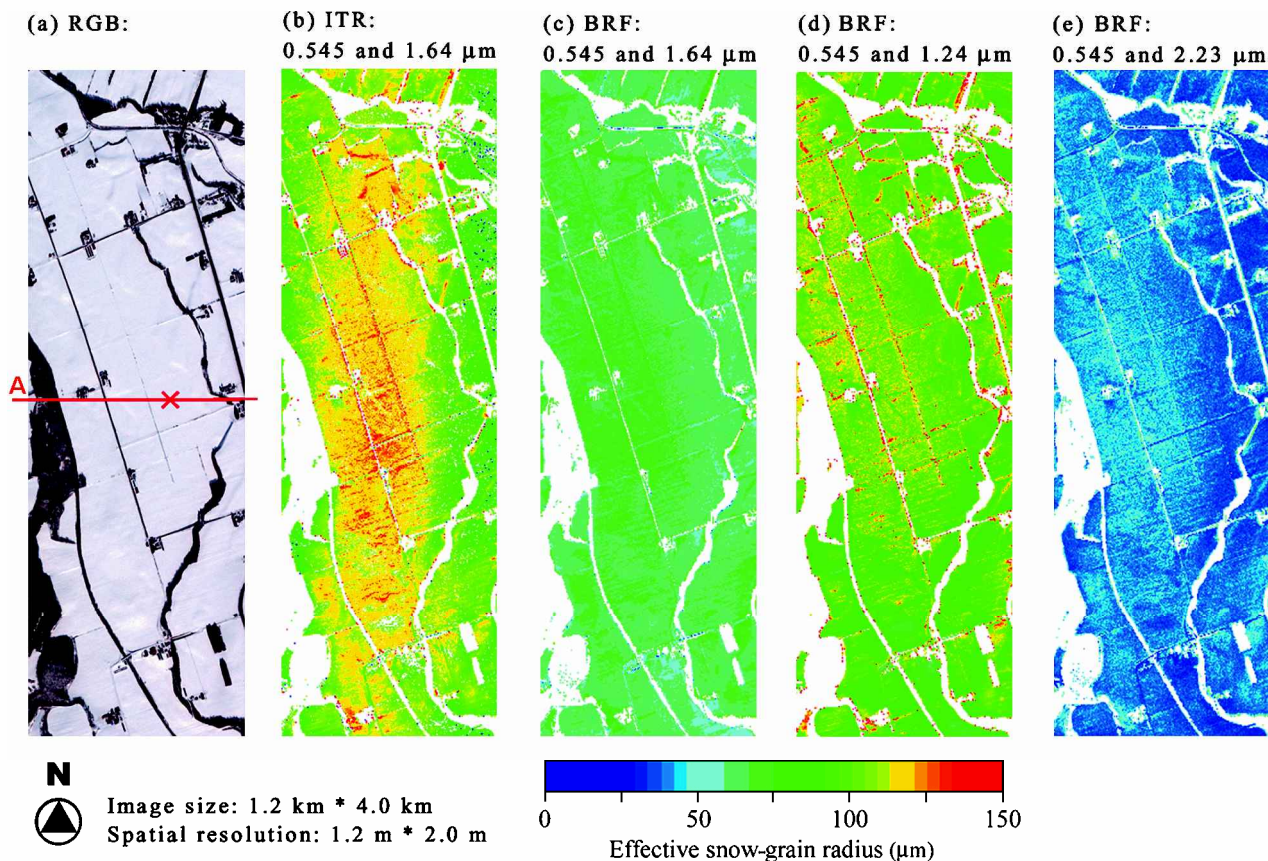


Fig. 5. (a) RGB composite image observed with AMSS. A cross indicates the site of the snow-pit work shown in Figure 4. Parameters at the pixels along line A are discussed in Figures 6 and 7. Swath is 1.2 km (east–west), and the observation distance (north–south) is 4.0 km. (b, c) Effective snow-grain radius retrieved from the AMSS data with the channel combination of “ $\lambda = 0.545$ and $1.64 \mu\text{m}$ ” using the isotropic reflectance (ITR) model and the BRDF model, respectively. (d, e) Same as (c), but retrieved from the channel combinations of “ $\lambda = 0.545$ and $1.24 \mu\text{m}$ ” and “ $\lambda = 0.545$ and $2.23 \mu\text{m}$ ”, respectively.

width of the dendrites (r_2) from the comparison between the measured spectral albedo and the theoretically calculated one. The concentration of snow impurities in the 0–5 cm layer was 5.2 ppmw, which was higher than that in the 5–10 cm layer, with 0.84 ppmw. From the electron micrograph of the impurities, the spherical particles and coagulated particles were recognized. Aoki and others (2000) mentioned that these particles may be dust (soil particle) and soot, respectively.

DEFINITION OF BRDF

BRDF at wavelength λ is defined by the upward reflected radiance $I(\theta_v, \phi_v, \lambda)$ from the snow surface contributed only by direct solar beam and the incident flux $F_0(\theta_0, \phi_0, \lambda)$ (on the surface normal to the beam) given by Warren (1982):

$$\text{BRDF}(\theta_0, \theta_v, \phi_0, \phi_v, \lambda) = \frac{I(\theta_v, \phi_v, \lambda)}{\mu_0 F_0(\theta_0, \phi_0, \lambda)}, \quad (1)$$

where (θ_0, ϕ_0) are incoming solar zenith and azimuth angles; $\mu_0 = \cos \theta_0$; and (θ_v, ϕ_v) are outgoing (reflected) zenith and azimuth angles. Since the observed snow surface was completely flat and free of azimuthally oriented features, the snow reflectance was assumed to depend on the relative azimuth angle between the viewing direction and the solar direction. Consequently, two variables (ϕ_0, ϕ_v) of BRDF can be replaced by azimuth difference $\Delta\phi = \phi_0 - \phi_v$. As AMSS observes the reflected radiance contributed from direct solar beam and downward diffuse radiation, it is impossible to

observe the BRDF defined by Equation (1) under the field observation with AMSS. Therefore, we assumed BRDF as defined by the upward reflected radiance $I(\theta_0, \theta_v, \Delta\phi, \lambda)$ from the snow surface to direct and diffuse illuminations and the downward solar flux $F(\theta_0, \lambda)$:

$$\text{BRDF}(\theta_0, \theta_v, \Delta\phi, \lambda) \sim \frac{I(\theta_0, \theta_v, \Delta\phi, \lambda)}{F(\theta_0, \lambda)}. \quad (2)$$

To compare with the snow isotropic reflectance that is described later, we used bidirectional reflection factor (BRF) given by:

$$\text{BRF}(\theta_0, \theta_v, \Delta\phi, \lambda) = \pi \text{BRDF}(\theta_0, \theta_v, \Delta\phi, \lambda). \quad (3)$$

The merit of BRF is that it is a dimensionless value normalized by the multiplication by π .

SNOW BRDF MODEL AND RETRIEVAL ALGORITHM

Theoretical snow BRDFs at visible and near-infrared wavelengths were calculated using a multiple scattering radiative transfer model for the atmosphere–snow system. Radiative transfer calculation assumes that snow grains consist of spherical particles and are based on the Mie theory for single scattering and the “doubling and adding method” for multiple scattering, omitting polarization (Aoki and others, 1999, 2000). According to Aoki and others (2000), smooth phase function such as Henyey–Greenstein (HG) is more suitable than the Mie phase function to simulate the BRDF of the snow surface. So we calculated BRDF using the HG phase function obtained from the asymmetry factor as in the Mie theory.

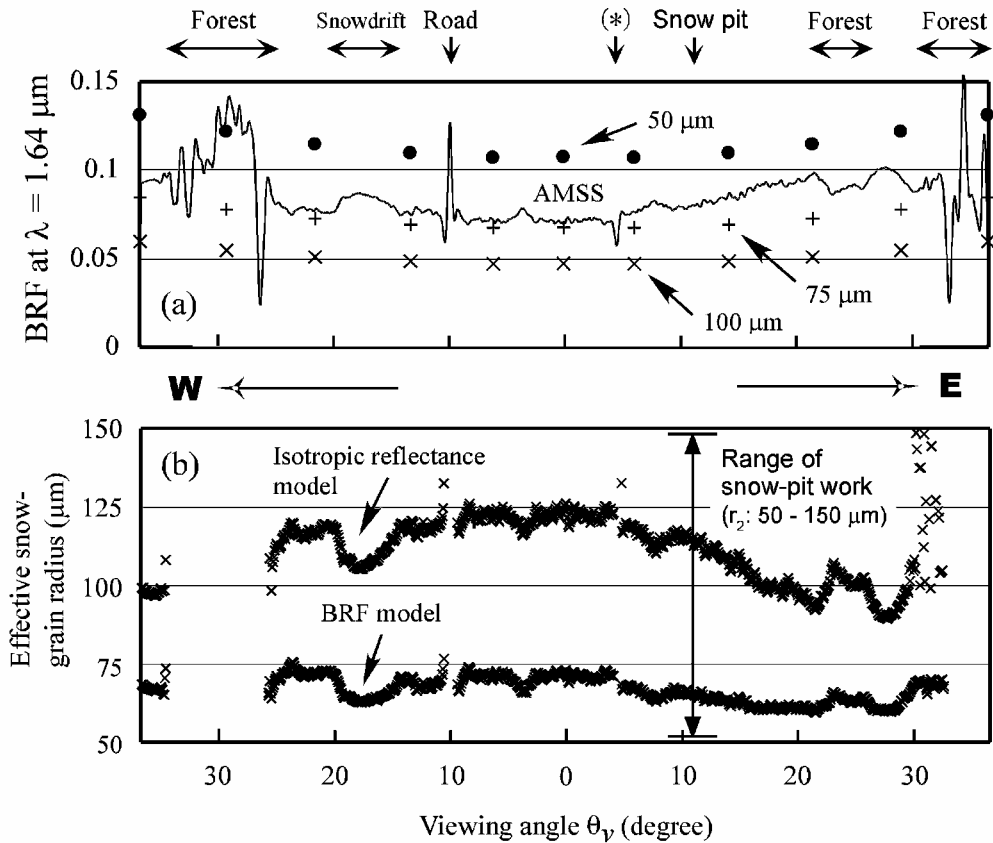


Fig. 6. (a) The theoretically calculated BRFs at $\lambda = 1.64 \mu\text{m}$ for $r_{\text{eff}} = 50, 75$ and $100 \mu\text{m}$ with the soot concentration of 0.1 ppmw , and the observed BRF with AMSS along line A in Figure 5a. The calculated BRFs are indicated by the characters \bullet , $+$ and \times , and the observed BRF is indicated by a solid line. (*) indicates “irrigation canal”. (b) Retrieved effective snow-grain radii along line A in Figure 5a using the ITR model and the BRF model.

The values of BRFs varied as functions of effective snow-grain radius and concentration of snow impurities. The refractive indices of ice used to calculate the snow BRFs were taken from the data compiled by Warren (1984) and Kou and others (1993). The types of snow impurities were assumed to be a dust-like model (United States Air Force, 1985) and a soot model (United States Air Force, 1985); these impurities are, respectively, weak and strong absorbers, mixing with snow particles as an external mixture as in Warren and Wiscombe (1980). The reason we assumed these to be the external mixture is that, in general, clean snow is carried by the north wind from the Sea of Okhotsk (Fig. 2) where there is no source of impurities. There are many farms around the observation site, hence the snow could be polluted with a dry deposition of local soil particles rather than soot.

The method of our algorithm for retrieving snow grain-size and the concentration of snow impurities is based on the look-up tables of the BRF at the visible and near-infrared wavelengths. The table was calculated for different snow grain-sizes, concentrations of snow impurities, viewing angles ($\phi_v = 0 \pm 35^\circ$) and azimuth angles. Solar geometric conditions are the same as those with the AMSS observation, where $\theta_0 = 53.5^\circ$ and $\Delta\phi = \pm 90^\circ$. We used the channels at $\lambda = 0.545 \mu\text{m}$ for the visible and $\lambda = 1.24, 1.64$ and $2.23 \mu\text{m}$ for the near-infrared regions. Atmospheric correction at each wavelength was not made, for two reasons: (1) the atmospheric effect at a flying height of 930 m is considered to be negligible; and (2) for the near-infrared regions, the effect of Rayleigh scattering would be weak. Although Rayleigh scattering is influenced by the atmospheric effect in the visible region, the BRDF pattern is not so anisotropic. Accordingly, the effect of Rayleigh scattering on the BRDF pattern in the

visible region would be weak. Figure 4 shows the relationship between BRF at $\lambda = 0.545 \mu\text{m}$ and BRF at $\lambda = 1.64 \mu\text{m}$ at $\theta_0 = 53.5^\circ$ which are the same as those of the AMSS observation. The values of BRFs decrease with the increase in snow grain-size and snow impurities, and vary with the viewing angle at $\theta_v = 0^\circ$ through 35° . When the reflectance at visible and near-infrared channels is determined from the AMSS data, the effective snow grain-size and snow impurities can be retrieved from the corresponding BRF look-up tables. For example, in Figure 4a, when the measured values of the

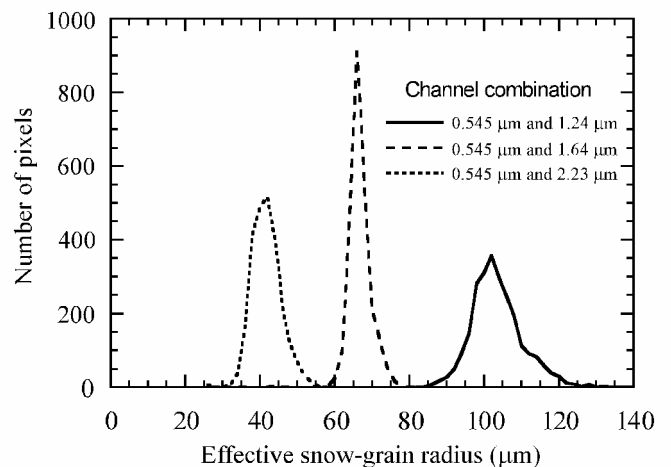


Fig. 7. Histograms of retrieved effective snow-grain radius from the AMSS data with the channel combinations of “ $\lambda = 0.545$ and $1.24 \mu\text{m}$ ”, “ $\lambda = 0.545$ and $1.64 \mu\text{m}$ ” and “ $\lambda = 0.545$ and $2.23 \mu\text{m}$ ” in the area of 2500 (50×50) pixels around the cross indicated in Figure 5a.

AMSS are 0.05 at $\lambda = 1.64 \mu\text{m}$ and 0.88 at $\lambda = 0.545 \mu\text{m}$ at $\theta_v = 0^\circ$, the effective snow-grain radius and the concentration of impurities of dust-like particles can be retrieved as $100 \mu\text{m}$ and 10 ppmw, respectively.

To verify the BRDF model, the retrieved snow grain-size from the algorithm using the BRDF model was compared with that from the algorithm using the isotropic reflectance model. The isotropic reflectance $\alpha(\theta_0, \lambda)$ is calculated by:

$$\alpha(\theta_0, \lambda) = \frac{1}{\pi} \int_0^{2\pi} \int_0^{\pi/2} \text{BRF}(\theta_0, \theta_v, \Delta\phi, \lambda) d\theta_v d(\Delta\phi). \quad (4)$$

In the BRDF (BRDF) and isotropic reflectance models, spherical ice particles were assumed, while the surface snow condition was faceted crystals (Fig. 3). According to Aoki and others (2000), the optically equivalent snow grain-size for the calculation of snow albedo by spherical ice particles is of the order of a branch width of dendrites or of a dimension of the narrower portion of broken crystals. However, for the BRDF of the snow surface consisting of non-spherical ice particles such as faceted crystal, further studies are necessary.

RESULT AND DISCUSSION

Effects of BRDF

The AMSS channels were chosen for $0.545 \mu\text{m}$ of the visible and $1.64 \mu\text{m}$ of the near-infrared. The reason for using the channel at $1.64 \mu\text{m}$ for the near-infrared is that snow is more anisotropically reflective at $\lambda = 1.64$ and $2.23 \mu\text{m}$ than at shorter wavelengths (Aoki and others, 2000), and the signal-to-noise ratio of the AMSS data at $\lambda = 1.64 \mu\text{m}$ is better than that at $\lambda = 2.23 \mu\text{m}$.

The RGB composite image observed with the AMSS is shown in Figure 5a. The results of effective snow-grain radius retrieved from the AMSS using the isotropic reflectance model and the BRDF model are shown in Figure 5b and c, respectively. In this figure, white areas indicate forests, houses, roads and irrigation canals, which were masked using the difference in normalized-difference vegetation index between snow and other surfaces (Saito and Yamazaki, 1999). However, these areas would not be masked completely due to the mixture with snow. The retrieved effective snow-grain radii using the isotropic reflectance model (Fig. 5b) are generally larger than those obtained from the BRDF model (Fig. 5c) in a widespread area of the AMSS image, because the isotropic reflectance is higher than the BRDF around nadir.

The observed and calculated BRDFs for pixels along line A of the AMSS image in Figure 5a are shown in Figure 6a. The observed BRDF of snow surface with the AMSS at $\lambda = 1.64 \mu\text{m}$ is higher at the viewing angle $\theta_v = \pm 35^\circ$ than at $\theta_v = 0^\circ$. This tendency is well simulated by the BRDF model, while the isotropic reflectance is constant for θ_v . If the snow surface is assumed to be uniform across the AMSS field of view, the retrieved snow grain-size would be a constant, independent of viewing angle. The retrieved effective snow grain-size (Fig. 6b) using the BRDF model was in a narrow range of $60\text{--}74 \mu\text{m}$ for the field. Using the isotropic reflectance model, grain-size varied widely, ranging from 89 to $125 \mu\text{m}$. On the other hand, the ground-truth data (snow-pit work) show that the measured snow-grain radius (r_2) at the surface layer ranged from 50 to $150 \mu\text{m}$ as shown in Figure 3. The effective snow-grain radii retrieved from the AMSS

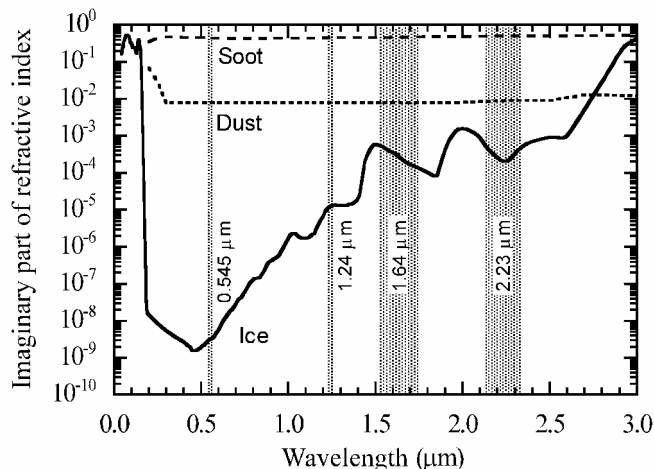


Fig. 8. Imaginary parts of refractive index of ice, dust-like model and soot model. The stippled rectangles indicate the half-width of each AMSS channel.

data using the two different models are $66 \mu\text{m}$ (BRDF) and $114 \mu\text{m}$ (isotropic reflectance) around the site of snow-pit work indicated by a cross in Figure 5a. These retrieved results are in the range of snow-pit work results ($50\text{--}150 \mu\text{m}$). However, the retrieved snow grain-size using the isotropic reflectance model was larger around the nadir than the edge of the image. This result is unnatural for the condition of flat snowfield where observation was made only 4 days after the snowfall. Thus, we can conclude that the algorithm to retrieve the snow grain-size using the BRDF model works well for the AMSS data.

Effective snow-grain radius and concentration of snow impurities retrieved from the AMSS data

The retrieved results of snow-grain radius using the BRDF model from the AMSS data with the channel combinations of “ $\lambda = 0.545$ and $1.24 \mu\text{m}$ ”, and “ $\lambda = 0.545$ and $2.23 \mu\text{m}$ ” are shown in Figure 5d and e, respectively. Comparing these results with Figure 5c, it can be pointed out that the snow grain-size becomes smaller when using the channels of longer wavelengths in the near-infrared region. The histograms of the retrieved snow grain-size in the area of $2500 (50 \times 50)$ pixels around the cross in Figure 5a are shown in Figure 7. The retrieved snow grain-size is smallest when using the channel of $2.23 \mu\text{m}$, and is largest with $1.24 \mu\text{m}$. This can be explained by the difference in absorptivity of ice. Figure 8 shows the imaginary part of the refractive index of ice, which indicates the degree of absorption. Since the light absorption by ice is weaker at shorter wavelength in these three channels, the sunlight penetrates into deeper layers, and the reflected light conveys information on snow physical parameters from a relatively deep layer. For the channels at longer wavelengths, the light absorption is stronger, and reflected light contains information from the top layer. On the other hand, the results of snow-pit work (Fig. 3) show that the measured snow grain-sizes at the surface are smaller than those at the deeper layers. Thus, the effective snow-grain radius retrieved from the AMSS data of different near-infrared channels are related with the vertical profile of snow grain-size. Li and others (2001) demonstrated the effect of photon penetration depth in the model calculation as the e-folding flux attenuation depth at wavelengths of $0.86, 1.05, 1.24$ and $1.73 \mu\text{m}$. Their theoretical results showed

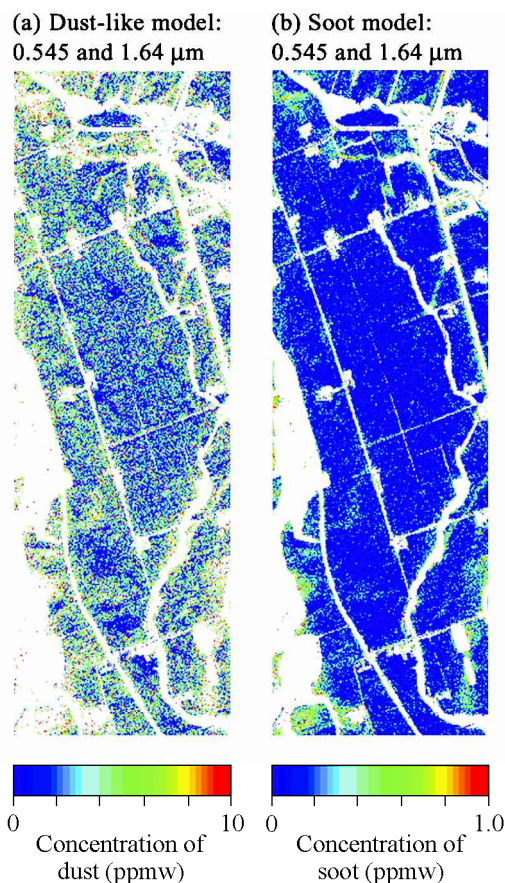


Fig. 9. The concentration of snow impurities (a) using dust-like and (b) using soot particles with the BRDF model. The AMSS channel was “ $\lambda = 0.545$ and $1.64 \mu\text{m}$ ”.

that photons with longer wavelengths penetrate less deeply into snow than those with shorter wavelengths, and therefore longer wavelengths carry information for a shallower layer of the snow. Our field results are congruent with the theoretical work of Li and others (2001).

Figure 9a and b show the concentrations of snow impurities retrieved from the AMSS data using the two kinds of snow-impurity models, in which dust-like and soot are weak and strong absorbers, respectively, as shown in Figure 8. The results of snow impurities retrieved from the AMSS data were about 2–5 ppmw for the dust-like model and 0.0–0.2 ppmw for the soot model. Since our observation site is in a rural area, it is possible that snow was polluted with a dry deposition of local soil particles rather than soot. The concentration of snow impurities measured from snow-pit work on 25 February 1998 was 5.2 ppmw in the layer 0–5 cm (Fig. 3). Moreover, in the electron micrograph analysis of the sampled snow impurities, many soil particles with a small amount of soot particles were observed. The absorption of general soil particles is similar to that of the dust-like model. Therefore, our retrieved results of snow impurities were roughly consistent with the results of snow-pit work. The results using the dust-like model suggest that the snowpack was contaminated with the external mixture of soil particles.

CONCLUSION

We developed the algorithms which take into account the snow anisotropic reflectance and retrieved snow grain-size and the concentration of snow impurities using the BRDF model from the AMSS data. The retrieved results of snow

grain-size and snow impurities are consistent with those of ground-truth data. In particular, the different near-infrared channels of AMSS were found to contain the information on the vertical profile of snow grain-size.

In this study, we used a one-snow-layer model to calculate the look-up table of snow BRF. However, snow is generally inhomogeneous in the vertical direction. This effect should be considered in the future. The anisotropic reflectance property of snow surface is more significant for the forward scattering direction. This correction is also an important issue for the remote sensing of snow.

ACKNOWLEDGEMENTS

We would like to thank M. Aniya (University of Tsukuba, Japan) and M. Ishizaki (Nano-electronics Research Institute, Japan) for invaluable discussion and advice. This work was conducted as part of the ADEOS-II/GLI Cal/Val experiments supported by the National Space Development Agency of Japan.

REFERENCES

- Aoki, T. and 6 others. 1998. Spectral albedo observations on the snow field at Barrow, Alaska. *Polar Meteorol. Glaciol.*, **12**, 1–9.
- Aoki, T., T. Aoki, M. Fukabori and A. Uchiyama. 1999. Numerical simulation of the atmospheric effects on snow albedo with a multiple scattering radiative transfer model for the atmosphere–snow system. *J. Meteorol. Soc. Jpn.*, **77** (2), 595–614.
- Aoki, T., T. Aoki, M. Fukabori, A. Hachikubo, Y. Tachibana and F. Nishio. 2000. Effects of snow physical parameters on spectral albedo and bi-directional reflectance of snow surface. *J. Geophys. Res.*, **105** (D8), 10,219–10,236.
- Bourdelle, B. and M. Fily. 1993. Snow grain-size determination from Landsat imagery over Terre Adélie, Antarctica. *Ann. Glaciol.*, **17**, 86–92.
- Fily, M., B. Bourdelle, J.-P. Dedieu and C. Sergent. 1997. Comparison of in situ and Landsat thematic mapper derived snow grain characteristics in the Alps. *Remote Sensing Environ.*, **59** (3), 452–460.
- Grenfell, T. C., S. G. Warren and P. C. Mullen. 1994. Reflection of solar radiation by the Antarctic snow surface at ultraviolet, visible, and near-infrared wavelengths. *J. Geophys. Res.*, **99** (D9), 18,669–18,684.
- Jordan, R. 1991. A one-dimensional temperature model for a snow cover: technical documentation for SNTherm.89. *CRREL Spec. Rep.* 91-16.
- Kou, L. H., D. Labrie and P. Chýlek. 1993. Refractive indices of water and ice in the 0.65 to 2.5 μm spectral range. *Appl. Opt.*, **32** (19), 3531–3540.
- Li, W., K. Stamnes and B. Chen. 2001. Snow grain size retrieved from near-infrared radiances at multiple wavelengths. *Geophys. Res. Lett.*, **28** (9), 1699–1702.
- Nolin, A. W. and J. Dozier. 1993. Estimating snow grain size using AVIRIS data. *Remote Sensing Environ.*, **44** (2–3), 231–238.
- Nolin, A. W. and J. Dozier. 2000. A hyperspectral method for remotely sensing the grain size of snow. *Remote Sensing Environ.*, **74** (2), 207–216.
- Nolin, A. W. and S. Liang. 2000. Progress in bidirectional reflectance modeling and applications for surface particulate media: snow and soils. *Remote Sensing Rev.*, **18**, 307–342.
- Saito, A. and T. Yamazaki. 1999. [Characteristics of spectral reflectance for vegetation ground surface with snow-cover, vegetation indices and snow indices]. *J. Jpn Soc. Hydrol. Water Res.*, **12** (1), 28–38. [In Japanese.]
- Sydor, M., J. A. Sorensen and V. Shuter. 1979. Remote sensing of snow albedo for determination of dustfall. *Appl. Opt.*, **18** (21), 3574–3578.
- United States Air Force. 1985. *Handbook of geophysics and the space environment*. Hanscom, United States Air Force, Air Force Geophysics Laboratory.
- Warren, S. G. 1982. Optical properties of snow. *Rev. Geophys. Space Phys.*, **20** (1), 67–89.
- Warren, S. G. 1984. Optical constants of ice from the ultraviolet to the microwave. *Appl. Opt.*, **23** (8), 1206–1225.
- Warren, S. G. and A. D. Clarke. 1986. Soot from Arctic haze: radiative effects on the Arctic snowpack. *World Data Center A for Glaciology (Snow and Ice)*, Boulder, CO, Glaciological Data 18, 73–77.
- Warren, S. G. and W. J. Wiscombe. 1980. A model for the spectral albedo of snow. II. Snow containing atmospheric aerosols. *J. Atmos. Sci.*, **37** (12), 2734–2745.
- Wiscombe, W. J. and S. G. Warren. 1980. A model for the spectral albedo of snow. I. Pure snow. *J. Atmos. Sci.*, **37** (12), 2712–2733.